Neurons protect themselves by active shrinkage upon axonal transection

Mehmet Şerif Aydın[1]†, Sadık Bay[1]†, Esra Nur Yiğit[1], Cemil Özgül[1], Elif Kaval Oğuz[6], Elçin Yenidünya Konuk[7], Neşe Ayşit[1,5], Nureddin Cengiz[8], Ender Erdoğan[9], Aydın Him[10], Mehmet Koçak[2,3], Emrah Eroğlu[1] & Gürkan Öztürk[1,4*]

Affiliations:

[1]Regenerative and Restorative Medicine Research Center (REMER), Research Institute for Health Sciences and Technologies (SABITA), Istanbul Medipol University; Istanbul, 34810, Türkiye.

[2]Biostatistics and Bioinformatics Analysis Unit, Research Institute for Health Sciences and Technologies (SABITA), Istanbul Medipol University; Istanbul, 34810, Türkiye.

[3]Department of Biostatistics and Medical Informatics, International School of Medicine, Istanbul Medipol University; Istanbul, 34810, Türkiye.

[4]Department of Physiology, International School of Medicine, Istanbul Medipol University; Istanbul, 34810, Türkiye.

[5]Department of Medical Biology and Genetics, School of Medicine, Istanbul Medipol University; Istanbul, 34810, Türkiye.

[6]Department of Science Education, Faculty of Education, Yüzüncü Yıl University; Van, 65080, Türkiye.

[7]Department of Medical Biology, School of Medicine, Bakırçay University; İzmir, 35665, Türkiye.

[8]Department of Histology and Embryology, School of Medicine, Bandırma Onyedi Eylül University; Bandırma, Balıkesir 10200, Türkiye.

[9]Department of Histology and Embryology, School of Medicine, Selçuk University; Konya, 42130, Türkiye.

[10]Department of Physiology, School of Medicine, Bolu Abant İzzet Baysal University; Bolu, 14030, Türkiye.

*Corresponding author. Email: gozturk@medipol.edu.tr

†These authors contributed equally to this work

Keywords: Axotomy, cytotoxic swelling, neurotrauma, axonal injury, neuron survival

Abstract:

Trauma, vascular events or neurodegenerative processes can lead to axonal injury and eventually transection (axotomy). Excessive water entry into injured neurons poses a particular threat since it may result in cytotoxic swelling and death. Neurons can survive axotomy, yet the underlying mechanisms are not fully understood. Using *in vitro* and *in vivo* neurotrauma model systems based on laser transection we demonstrated that axotomy triggers actomyosin contraction coupled with calpain activity. As a consequence, neurons shrink acutely to force water through aquaporin channels preventing swelling and burst. Inhibiting shrinkage increases the probability of death of injured neurons by about three fold. This study reveales a first-line cytoprotective response mechanism to neurotrauma and offers a fresh perspective on pathophysiological processes in the nervous system.

Introduction

The axons of most neurons sometimes extend to several thousand-fold lengths of the cell's diameter. Such a prominent structure represents a substantial cellular surface area susceptible to intrusions of various kinds, ranging from traumas to autoimmunity. Many nervous system disorders start or progress by axonal injury, which may result in the death of the affected neuron, acutely or over extended periods. In the aftermath of an axon transection (axotomy), the neuron becomes susceptible to Na^+, Cl^-, and Ca^{++} influx through the cut-end until effective sealing. Especially in injuries close to the neuronal body, ion influx happens through specific channels in the soma that open due to a change in the electrical potential of the plasma membrane or mechanical stimuli caused by the injury. Water accompanies ions into the neuron as cytosol becomes more and more hyperosmolar (*1, 2*). Two main mechanisms are known to decrease solute load and reduce the risk of swelling after axonal injury. First, during strong depolarization created by axonal injury, the Na^+-Ca^{++} exchange pump is tuned to pump out highly accumulated Na^+ in exchange for Ca^{++} (*3, 4*). However, this may dangerously elevate cytosolic Ca^{++}, potentially triggering destruction in the plasma membrane, mitochondria, and cytoskeleton (*4*). Another acute response is to reduce intracellular Cl^- load by co-transport with K^+ out of the neuron, which may over-activate the Na^+-K^+ ATPase to reuptake K^+ into the cell, contributing to an imminent energy crisis (*2, 5, 6*).
Laser axotomy *in vitro* and in living animals is an established method for examining the factors influencing neuronal survival and degenerative processes. We observed a hitherto unreported phenomenon during laser axotomy tests: *shrinkage in neuronal soma*. This critical discovery aligns with earlier findings that neurons employ local axonal contractions to promote sealing cut axon ends (7). We hypothesized that actomyosin contraction in the neuronal body might be a component of the initial response to axotomy counteracting swelling.

Results & Discussion

Axotomy causes significant cell size reduction, preceded by membrane depolarization and calcium influx

Using high-resolution microscopy, the *in vitro* experimental paradigm employs time-lapse imaging of adult primary sensory neurons during the transection of outgrown axons with a laser beam at physiological temperature and atmosphere. In response to laser axotomy, neurons immediately started to shrink. Cell surface area change analysis unveiled that the neuron's body shrunk about 12% within the first 15 minutes (Fig. 1A, B, and movie S1). Notably, about half of the shrinkage happened during the first 5 minutes, which we selected as the reference time point for other experiments. Next, we sought to understand this observation's physiological relevance and tested Thy1-GFP line M mice with sparse GFP expression in dorsal root ganglia (DRG) neurons (*8*), where individual axons can be identified, allowing precise *in vivo* laser transection. As described before, an imaging window exposing second lumbar (L2) DRG was surgically formed (*9*). With a femtosecond infrared laser of a two-photon microscope, we cut single axons and demonstrated that neurons *in vivo* shrunk comparable to isolated cells *in vitro* (Fig. 1A, B). In order to determine if shrinking also affects the central nervous system or exclusively primary sensory neurons, we also axotomized hippocampal neurons in culture. Compared to sensory neurons in the spinal cord, hippocampal neurons had a considerable but less dramatic size loss. Thus, we selected DRG neurons as a model system for the remainder of the study due to their excellent *in vitro* survival and the ease of intravital imaging. Axotomy causes membrane depolarization and action potentials in cortical neurons *in vitro* (*1*). Since many post-axotomy

events can be related to this and concurrent Ca^{++} influx, we first characterized these phenomena by patch-clamp recordings taken during axotomy and by Ca^{++} imaging using genetically encoded calcium sensor GCamp6 expressing DRG neurons. Laser axotomy significantly depolarized the membrane with or without generating action potentials (AP) (Fig. 1C). After 24 hrs, the resting membrane potentials of axotomized neurons were similar to the control values. However, when re-axotomized, the membrane potential depolarized comparable to naïve neurons but AP generation was seldom (Fig. 1D and supplementary text). Live-cell Ca^{++} imaging unveiled that cytosolic Ca^{++} levels rose sharply after axotomy and returned to baseline levels within an hour (Fig. 1E and movie S2). We also observed that if the proximal stump was not promptly sealed, Ca^{++} inflow persisted through it, leading to more cytosolic Ca^{++} accumulation (movie S3 and S4).

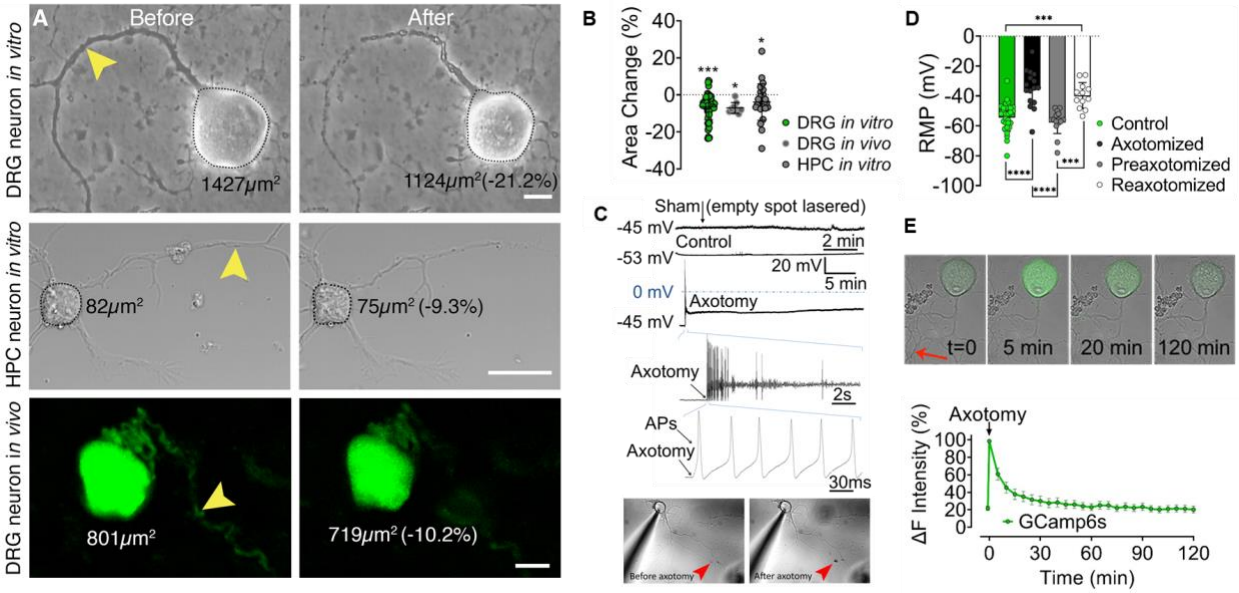

Fig. 1. Acute consequences of axotomy. (**A**) Images show dorsal root ganglion (DRG) and hippocampal (HPC) neurons *in vitro* and a DRG neuron of a live Thy1-GFP mouse before and after laser axotomy (scale bar, 15 µm; arrowhead points to the site of axotomy). (**B**) The scatter dot plot shows changes in the surface area in 5 mins following axotomy in cultured (n=6/65) and *in vivo* DRG neurons (n=3/9) and hippocampal neurons (n=3/25). Wilcoxon Signed Ranks Test was used to compare surface areas before and after axotomy (**C**) Membrane potential recordings from a control and an axotomized neuron. Images show simultaneous patch-clamp recording and axotomy (arrowhead points to the injury site). (**D**) Bars represent levels of the RMP of neurons before (n=4/29), immediately (n=3/16)), and 24 hrs (n=3/15) after axotomy and following the second axotomy (n=3/12); Kruskal Wallis and Mann-Whitney U tests were used to compare groups. (**E**) Real-time Ca^{++} traces upon axotomy in GCamp6-expressing neurons. Error bars: SEM; n=number of animals used/number of cells analyzed; for all tests: *p<0.05, ***p<0.0001, ****p<0.00001.

Calcium entry through voltage gated channels triggers actomyosin contraction.

Besides the cut axon tip, Ca^{++} may enter the cell through voltage-gated calcium channels (VGCCs). DRG neurons express five types of VGCCs: L, N, P/Q, R, and T-types (*10, 11*). Using pharmacological antagonists to inhibit these channels selectively, we unveiled that L- and N-type Ca^{++} channels made the earliest contribution to the shrinkage after axotomy. Their respective blockers nifedipine (NIF) or ω-conotoxin GVIA (CNX) effectively inhibited cell size reduction after axotomy (Fig. 2A). NIF-mediated inhibition was most effective in the first 5 minutes and became less uniform and statistically insignificant 15-60 mins, while CNX exerted a more

consistent inhibition. Blocking R-type channels with SNX-482 (SNX) effectively prevented shrinking after 15-60 mins post axotomy. Inhibition of P/Q type channels with ω -agatoxin-IVA (AGX) and T-type Ca^{++} channels with mibefradil (MIB) proved ineffective. Predominance of L and N type channels in the early stages of shrinkage and significant contribution of R type channels later on are consistent with a previous study in which they depolarized rat DRG neurons with high K^{+} and analyzed contribution of VGCCs to Ca^{++} influx (*11*). VGCCs are classified as either high or low-voltage-activated types. The level of their expression and expression ratio among subtypes of primary sensory neurons differ; these are subject to change in culture (*10, 12, 13*). Our findings demonstrate that Ca^{++} influx through the high-voltage-activated L-, N-, and R-type channels induce shrinking in cultured DRG neurons. The degree to which these observations accurately represent *in vivo* circumstances is yet unclear. Experiments with thapsigargin (TG) showed that release of internal Ca^{++} stores in the first few minutes after axotomy contributes to but not essential for the shrinkage but acts as a significant Ca^{++} resource later. In fact, forced release of Ca^{++} from internal stores by TG was enough to induce shrinkage in neurons even without axotomy (data not shown).

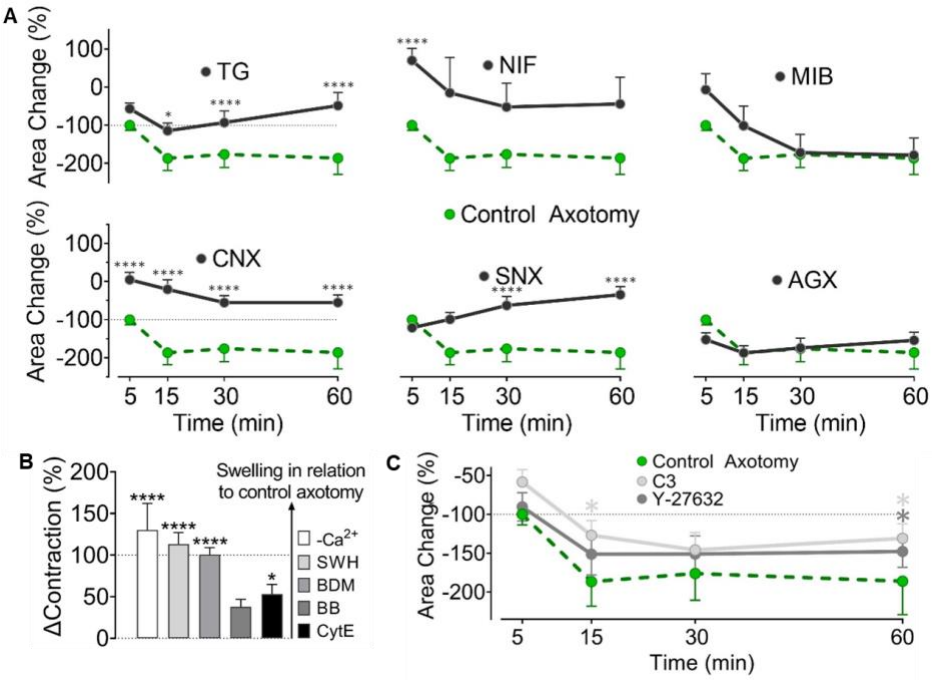

Fig. 2. Mechanisms of calcium elevation and actomyosin contraction after axotomy. (**A**) Effect of inhibition of voltage-gated calcium channels (VGCC) and internal Ca^{++} stores on surface area changes after axotomy. VGCC subtypes L, N, P/Q, R, and T, were blocked with nifedipine (NIF) (n=4/46), ω-conotoxin GVIA (CNX) (n=3/30), ω -agatoxin-IVA(AGX) (n=3/23), SNX-482(SNX) (n=3/18) and mibefradil (MIB) (n=3/28) respectively. Thapsigargin (TG) (n=4/44) was used to deplete internal Ca^{++} stores before axotomy. **(B)** Effect of inhibition of actomyosin contraction on surface area change 5 mins after axotomy in Ca^{++}-free medium (n=3/38), myosin inhibitors butanedione monoxime (BDM (n=3/30)) and blebbistatin (BB) (n=4/48) and actin inhibitors cytochalasin E (CytE) (n=3/33) and swinholide A (SWH) (n=3/41). The data are normalized relative to control axotomy (baseline) and presented as mean ± SEM for easier interpretation; the taller the bar, the more potent the inhibition of shrinkage. **(C)** Effect of inhibition of RhoA signaling with clostridium botulinum exoenzyme C3 (n=3/20) or RhoA's effector ROCK with Y-27632 (n=3/30) on surface area change after axotomy. Mann-Whitney U test was used to compare surface area changes in each group to the changes 5 mins (B) or at indicated time points (A, D)

after control axotomy (n_5=6/65, n_{15}=6/28, n_{30}=6/43, n_{60}=6/60). Error bars: SEM; n=number of animals used/number of cells analyzed; for all tests: *p<0.05, ****p<0.00001.

We then hypothesized that Ca^{++} - induced active contraction and cytoskeleton reshaping might be responsible for the cell shrinkage. To verify this, we first conducted *in vitro* axotomies in Ca^{++} - free medium or in the presence of inhibitors of actin (cytochalasin E -CytE and swinholide A - SWH) or myosin (blebistatin – BB and 2,3-Butanedione monoxime- BDM). Lack of extracellular Ca^{++} and addition of SWH, CytE, and BDM significantly inhibited neuronal shrinkage while BB proved ineffective (Fig. 2B). CytE prevents polymerization of actin while SWH severs f-actins (14, 15). CytE exhibited a less significant effect than SWH, indicating that part of the contraction may still be mediated by the pre-existing f-actins even while the production of new polymers was inhibited. Failure of BB to counteract the shrinkage may be due to its high selectivity against myosin subtypes (16). However, BDM, a more general myosin inhibitor, which blocks phosphorylation of myosin light chain (MLC) kinase (17) effectively prevented the size reduction.

RhoA signaling is not essential but contributes to the actomyosin contraction.

We next focused on signaling mechanisms regulating the Rho GTPases and their downstream effectors, Rho-associated kinases (ROCKs). In non-muscle cells, such as neurons, the Rho GTPases and their downstream effectors, Rho-associated kinases (ROCKs), govern actomyosin contractility in a Ca^{2+} dependent manner (18, 19). We performed axotomy in the presence of RhoA inhibitor exoenzyme C3 and ROCK inhibitor Y-27632. Cell shrinkage was significantly reduced by inhibiting RhoA within 15 minutes and inhibiting RhoA or ROCK after 60 minutes post axotomy (Fig. 2C). Y-27632 displayed marginal effects; possibly because ROCK enhances actomyosin contraction only through MLC. However, RhoA has an additional effector, diaphanous-related formin 1 (mDia1), which activates profilin, an actin-polymerizing and stabilizing factor (*20*). The endothelial cell stretch model demonstrated a similar temporal relationship among Ca^{++} increase, RhoA activation, and actomyosin contraction (*21*). Our data indicate that RhoA activation contributes not immediately but minutes after axotomy and is only partially responsible for actomyosin contraction. We propose that the likely mechanism starts with membrane depolarization induced by axotomy, followed by Ca^{++} influx that directly triggers the contraction and activates RhoA system, which comes in later and contributes to the process by increasing actin polymers and disinhibiting MLC.

Calpains digest cytoskeleton to enable shrinkage.

An actomyosin cortex lies beneath the plasma membrane and, with its capacity to contract, involves various cellular events from cell morphology to the regulation of intracellular hydrostatic pressure (*22*). However, the tension created by contraction should overcome the opposing forces exerted by relatively static structural elements of the cytoskeleton. At this point, we thought that axotomy might cause the activation of proteolytic enzymes, namely calpains, which could break down cytoskeleton elements and reduce the opposing forces. To test this hypothesis, we axotomized cultured neurons in the presence of a general calpain inhibitor PD150606 (PD) and found that this approach almost completely prevented cell shrinkage (Fig. 3A). Calpains are activated by increased intracellular $Ca^{++,}$ targeting many functional and structural proteins, which make them accountable for various pathological changes in neurodegenerative processes (*23, 24*). Although we did not experimentally identified, the likely substrates of calpains may be spectrin, which forms a pre-tensed supporting mesh beneath the plasma membrane and tubulin, which constitutes the major solid network opposing the compression forces (*24, 25*). On the other hand, actin and myosin are reported not to be among the primary targets of calpains (*26*). Thus, during

the inhibition of calpains, actomyosin contraction can still occur, but neurons cannot shrink due to the resistance of the intact cytoskeleton. The cell could not avoid swelling when actomyosin contraction is prevented in addition to calpain activity. This observation needs further explanation since BDM alone did not cause swelling. It is possible that beside obvious cytoskeletal substrates, calpains' contribution to the neuronal shrinkage may involve cleavage of some other proteins among its many other substrates from glutamate to calcium channels, which may influence water influx (26).

An isotonic contraction pumps water out of the axotomized neuron.

We next sought to understand whether the change in cell surface area after axotomy means a change in volume as the opposite is possible since neurons may get elongated vertically while shrinking laterally. We cultured DRG neurons from EGFP mice and acquired three-dimensional images with a fast confocal microscope during axotomy. In parallel with the change in surface area, neuronal volumes were significantly reduced (Fig. 3B, C, and movie S5). Next, with a special microscope combining a laser microdissection and an optical tweezer, we compared the membrane tension of neurons before and after axotomy (Fig. 3D). While the lateral tension significantly increased, axotomy did not affect the cortical membrane tension (Fig. 3E). A decreasing cell volume and only slightly elevated membrane tension clearly defined an isotonic type of contraction in agreement with the Law of Laplace (*27*). To explain the volume loss, we proposed that, by contraction, water may be extruded from the cells through aquaporin channels (AQP) (*28*). Indeed, when we blocked AQPs with $HgCl_2$, neuronal size did not change upon axotomy while the membrane tensions significantly increased; thus indicating transformation of contraction from isotonic to isometric type (Fig. 3E, F).

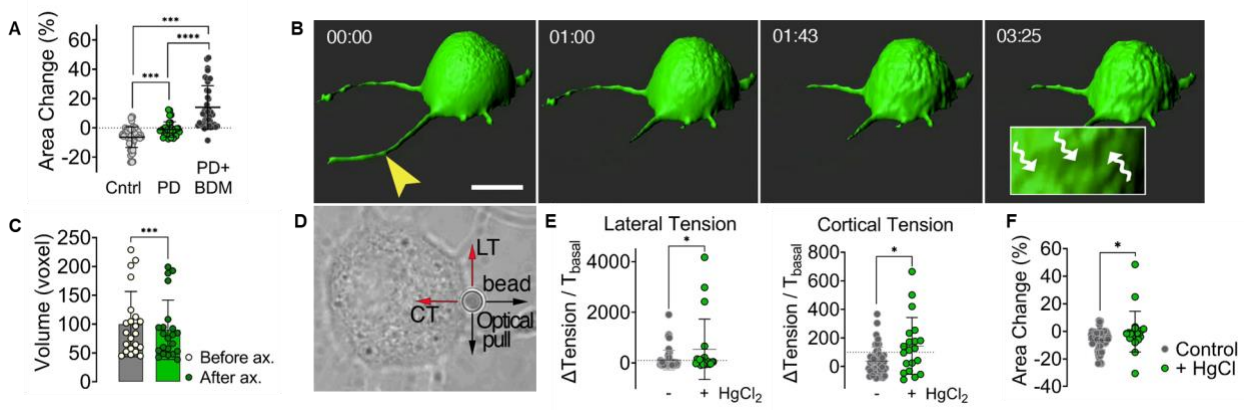

Fig. 3. Characteristics of axotomy–induced shrinkage. (A) Scatter dot blot shows surface area change 5 mins after axotomy in the presence of calpain inhibitor PD150606 (PD) alone (n=3/33), in combination with the myosin inhibitor butanedione monoxime (BDM) (dots, n=4/41) and control conditions (n=6/65). Kruskal Wallis (A) and Mann-Whitney U test was used for comparisons. **(B)** Representative three-dimensional confocal images show an axotomized neuron over time. Wavy arrows in the inlet point to depressions on the cell surface due to shrinkage (scale bar, 15 µm; arrowhead points to the site of axotomy). **(C)** Bars represent the mean volume change of axotomized DRG neurons 5 mins before axotomy (grey bar) or after axotomy (green bar) (n=3/22). Wilcoxon Signed Ranks Test was used to compare volumes before and after axotomy. **(D)** Representative bright-field image shows measurement of membrane tensions by pulling an attached polystyrene bead with optical tweezer. (**E)** Changes in the membrane tensions (T) due to axotomy (n=4/48) and the effect of aquaporin (AQP) channel inhibition with $HgCl_2$ (n=3/20) **(F)** Comparison of surface area change 5 mins after axotomy with AQP inhibition (n=3/20) to the control

axotomy (n=6/65). Mann-Whitney U test was used for comparisons. Error bars: SEM; n=number of animals used/number of cells analyzed; for all tests: *p<0.05, ***p<0.0001, ****p<0.00001.

Shrinkage increases survival chance of axotomized neurons *in vitro* and *in vivo*.

Our investigations thus far showed that neurons respond to axotomy by shrinking under the influence of actomyosin contraction and calpain activity , which forces water out of the cell through AQP channels. Thus, we hypothesized that shrinkage could help neurons survive by prevention of swelling. We ran several *in vitro* and *in vivo* experiments to test this hypothesis.

In culture, when contraction was inhibited by BDM, more neurons died progressively over 24 hrs incubation period (Fig. 4A and supplementary text). The surviving axotomized neurons for the next 1 and 24 hrs were those that had shrunk, and those that died had not shrunk by the 5th-minute post axotomy (Fig. 4B). The chance of survival after axotomy was correlated to the degree and persistence of shrinkage (fig. S1 and supplementary text). With *in vivo* experiments, we sought out the biological relevance of these *in vitro* findings suggesting that shrinkage is in favour of injured neurons. Using the same technique utilized for *in vivo* axotomy (9), we constructed an imaging window over L2 DRG of Tau - EGFP mice whose neuronal soma was brightly labeled (*29*). The basic experimental paradigm was to cut the peripheral nerve emanating from the DRG, thus axotomizing all neurons it holds. Propidium iodide (PI) was injected intravenously to monitor cell death. In some experiments, BDM was intrathecally administered prior to nerve cut. With a two-photon microscope, we took images before and 5 minutes, and 24 hrs after axotomy. The nerve cut caused an apparent reduction in size, which was even more significant after 24 hrs (fig S2). BDM prevented neuronal shrinkage and significantly increased neuronal death compared to control animals, while sham group with only BDM injection showed no neuron loss (Fig. 4C,D and fig S2). As in the *in vitro* experiments, surviving neurons were those that had shrunk. *In vivo* single-cell axotomy in Thy1-GFP animals did not shrink DRG neurons after BDM pre-injection (fig S2).

An interesting observation we made but not quantitatively analyzed in this study was that contraction of soma could amputate the proximal stump when axotomy is very close, which represents a very rapid and efficient way of membrane sealing, potentially increasing the chance of survival when the risk of death is more significant (movie S6).

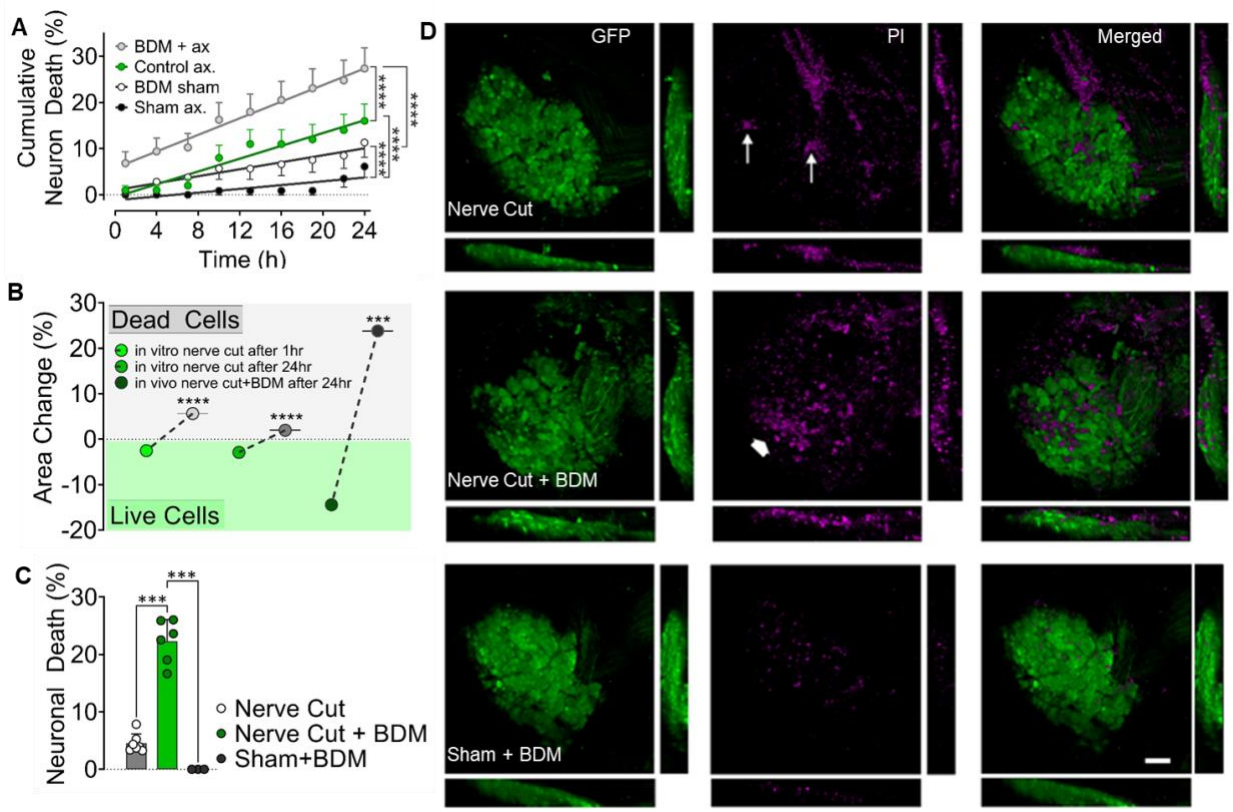

Fig. 4. Relationship of axotomy-induced contraction with neuronal survival. (A) Cumulative death rates of axotomized and control neurons during 24hrs incubation period with and without inhibition of actomyosin contraction by butanedione monoxime (BDM) (n=3/117 (BDM+ax), 3/100 (Control ax), 3/106 (BDM sham), 3/114 (Sham). Groups were compared using a Repeated-measures Mixed Model. **(B)** Surface area changes of neurons that survived and died after *in vitro* axotomy (n=16/303 (live 1 hr), 16/113 (dead 1 hr), 16/160 (live 24 hr), 16/266 (dead 24 hr)) and *in vivo* nerve cut (n=6/11 (live), 6/10 (dead)). Note that *in vitro* data were pooled from various experimental groups including those with pharmacological agents. Mann-Whitney U test was used for comparisons. **(C)** Rate of cell death in DRGs 24hrs after peripheral nerve cut or sham operation and effect of inhibition of actomyosin contraction with BDM *in vivo*. Comparison of neuronal death rates was performed with Kruskal Wallis and Mann-Whitney U tests, and the data are shown as mean ± SEM (n=7 (nerve cut), 6 (nerve cut+BDM), 4 (sham + BDM)). **(D)** Representative confocal images of DRGs from *in vivo* experiments in C. Arrows point to few PI-stained dead neurons while the thick arrow shows a large group of them (scale bar, 100 µm). Error bars: SEM; n=number of animals used/number of cells analyzed; for all tests: ***p<0.0001, ****p<0.00001.

Conclusion

This study describes an axotomy-induced actomyosin contraction coupled with proteolysis that shrinks injured neuron to pump out water, preventing an imminent swelling and death (Fig. 5). The axotomy-induced membrane depolarization that opens high voltage-activated Ca^{++} channels is the first step in the proposed processes. Increased cytoplasmic Ca^{++} triggers actomyosin contraction and activates calpain enzymes that break cytoskeletal proteins to reduce physical resistance against shrinkage. The contraction is partially sustained by RhoA signaling and occurs isotonically pumping water out of the cell through AQP channels.

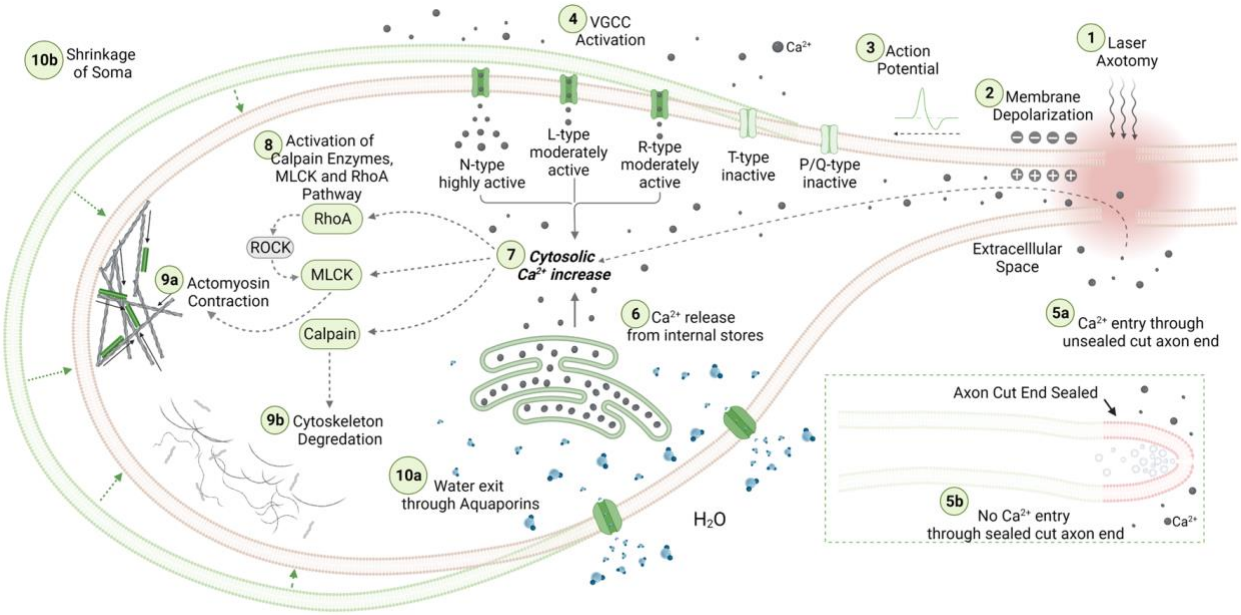

Fig. 5. Schematical overview of the involved mechanisms in cell shrinkage upon axotomy: See main text for a detailed description.

The tell-tale sign of this protective response is a reduction in somatic size, which was also reported by others both in central and peripheral neurons (*30-35*). This change was often considered atrophy and attributed to loss of function due to disconnection from the target. Although atrophy is a likely outcome of an axonal injury in the long term, shrinkage in cholinergic septal neurons 24 hrs and retinal ganglion neurons three days after axotomy may hardly be called atrophy (*33, 34*). In the existing literature, the contractile capacity of neurons has been chiefly associated with neurites and growth cones (*7, 36*). An exception relevant to our findings was a report by Wan et al. back in 1995, stating that "*a plasma membrane-linked contractile machinery (presumably actomyosin) might contribute to the neurons' mechano-osmotic robustness by restricting water influx*" during hyposmotic challenge (*37*). We have demonstrated that water leaves the shrinking neurons via AQP channels. AQP1 is expressed in DRG neurons and upregulated after nerve injury (*38*), and AQP2 expression is induced after nerve constriction (*39*). $HgCl_2$, by which we blocked water efflux, is primarily an AQP1 inhibitor but not strictly selective (*40*). Therefore, we do not exactly know which subtypes of AQPs are responsible for water efflux. We investigated the mechanism of shrinkage using mainly DRG neurons. We did not differentially analyze, but heterogeneity among different subtypes of these neurons in shrinkage response to axotomy can be expected due to varying constitutional expression of molecular components of the event. This heterogeneity is even more likely in central neurons, where we observed minor average size reduction with more significant deviations across individual cells. On the other hand, our observation that the initial size of DRG neurons, which roughly defines different subpopulations (*41*), does not affect the unique consequence of the shrinkage - the increased chance of survival- suggests that phenotypic differences do not preclude the significance of the phenomenon.

We believe that the interaction of shrinking neurons with neighbouring cells may have significant consequences like mechanical signaling (*42*).

In this study, we have revealed a critical phenomenon that protects neurons after axotomy. This mechanism may have far-reaching implications in various nervous system disorders, from direct traumas to neurodegenerative diseases associated with primary or secondary axonal injury.

Materials and Methods

Animals

Use of animals in this study was approved by Istanbul Medipol University Animal Experimentation Ethical Committee. Maximum care was paid to use the minimum number of animals necessary for the research aims and to minimize suffering throughout the study. All procedures were conducted in compliance with European Council Directive 2010/63/EU.

Breeding colonies of all mice strains were obtained from The Jackson Laboratory and bred at Istanbul Medipol University Experimental Animal Facility. These were general GFP - B6 ACTb-EGFP (stock no: 003291) (*43*), TauEGFP knock-in (stock no: 004779) (*29*), Thy1-GFP line M (stock no: 007788) (*8*), cross breeds of cre-dependent GCaMP6s - Ai96(RCL-GCaMP6s) (*44*) (stock no: 024106) and Vglut2-ires-cre (stock no: 016963) (*45*) and non-transgenic BALBc (stock no: 000651)mice.

Neuron cultures

Adult primary sensory neuron cultures

Dorsal root ganglia (DRG) were removed from adult mice and primary sensory neurons were isolated as described before (*46*). Briefly, animals were anesthetized with an I.P. injection of ketamin (Pfizer) and sacrificed by cervical transection. Vertebral column was cut out and quickly transferred into dissection plate with RPMI1640 medium (Sigma). DRGs were collected under a stereo microscope and digested by collagenase (Sigma, 100 U/ml, 50 min) and trypsin (Sigma, 1mg/ml, 15 min) treatments after which they were triturated through pipet tips of narrowing bores for 15 minutes and finally through a 26-gauge injector needle. The cell suspension obtained was treated with DNAse, spun at 120 g for 3 min and the pellet was resuspended in Neurobasal A supplemented with B27 (Thermo Fisher), glutamine (Glutamax-Thermo Fisher) and antibiotic solution (Sigma) (NBA-B27). To eliminate non neuronal cells, gradient centrifuge technique is used. The cell suspension was carefully pipetted on top of a three-layer percol (Sigma) gradient (60%, 35% and 10% from bottom to top) prepared in NBA-B27 and spun at 3000 g for 20 min in a centrifuge at 4°C. The neurons collected from 35% layer were washed with NBA-B27 and spun once more at 120 g for 3 min after which the supernatant was discarded and the pellet was resuspended in NBA-B27.The suspension was transferred on 35 mm diameter glass bottomed Petri dishes (WPI) coated with poly-L-lysine and laminin and incubated at 37°C with 5% CO_2.

Newborn hippocampal neuron cultures

Postnatal (p1-p3) mice were sacrificed with CO_2 and brains were collected under aseptic conditions. Hippocampi was surgically removed in dissection medium (L15, 1% antibiotic-antimycotic solution), cut into small pieces and digested with papain (Sigma, 12.5 U/ml, 45 min) with agitation at 4 ºC. Afterwards, the suspension was triturated via serial pipetting and papain was inhibited with 10 % FBS containing dissection medium for 15 min at 4 ºC. Then, cells were pelleted by centrifugation at 180 g for 5 min at 4 ºC, dissection medium was discarded and cells were plated on poly-D-lysine coated glass bottom culture dishes and incubated in NBA-B27 at 37°C with 5% CO_2.

Microscopic imaging and in vitro manipulations

For microscopic imaging, following systems (all from Zeiss) were used: LSM780 NLO, LSM880 and LSM7 MP laser scanning confocal and two photon microscopes, Cell Observer time-lapse imaging system and Palm Combi system. Various modules of Zeiss Axiovision and Zen software

were used for time lapse imaging of multiple positions at desired intervals, three-dimensional scanning, and Ca^{++} signal imaging. Axotomy was performed with the femtosecond infrared lasers of two-photon microscopes in vivo and UV lasers fitted to LSM880 and Palm laser microdissection - optical tweezer combi system in vitro.

In vitro axotomy

A brief pulse (0.5-1 sec) of UV (337nm or 355nm) laser beam was focused on axons about 50-100 µm distal to the soma emitting approximately 1–30 pulses per second, each lasting 3 nsec and delivering approximately 300 µJ of energy. For sham operations, an empty spot 50 µm away from the cell body was irradiated similarly.

Membrane tension measurement

The optical tweezer controlled by Palm software with force measurement module was used for membrane tension measurements. For this, poly-L-lysin-coated 3 µm-diameter polystyrene beads (Sigma) were carried and attached to the neuronal plasma membrane by the optical trap. Then they were pulled vertical or parallel to the plasma membrane with the optical trap to measure cortical and lateral membrane tensions respectively. The force resisting the pull was measured in piconewtons and reported by the software.

<u>In vivo experiments</u>

Vertebral window surgery

Construction of imaging window over lumbar DRGs was performed according to the method described by Chen et al. (*9*). Briefly, the mice were anesthetized with 2% isoflurane (30% O_2) and a small incision was made in the dorsal skin at the level of L1-L3 of the spine, paraspinal muscles and ligaments connected to right transverse processes of L1 to L3 were carefully dissected using fine scissors to expose DRG. The mouse was then placed lying on its left side onto custom-made vertebral holder which allows access to L2 DRG for in vivo microscopy. Carefully removing surrounding muscles and connective tissue around the L2 DRG using fine tweezer, DRG was exposed. To achieve optical clearance and stabilization, DRG and surrounding bone structures were covered with silicon adhesive Kwik-Sil® (World Precision Instruments), sealed with 3-mm diameter round cover glass. The cover glass was fixed to vertebrae using cyanoacrylate glue and dental cement.

Peripheral nerve cut

TauEGFP knock-in mice were used to perform axotomy in all neurons within the DRG by cutting the peripheral nerve of DRG. This strain was preferred for these experiments due to strong expression of EGFP in neuronal soma, which enabled deep imaging and analyzing surface area changes. Using the two-photon microscope (LSM 7MP), neurons in L2 DRG were imaged through the vertebral window with 10x/0.45NA air objective and 820nm excitation laser before and after its peripheral nerve was completely cut with surgical scissors.

In vivo axotomy

Thy1-GFP line M mice were preferred for single cell axotomy as seldom labelled DRG neurons with clearly visible axons were easier to identify and analyze after the procedure. Single cell axotomy was performed by irradiating axons with Ti:Sa laser about 100 µm distal to the cell body. For this purpose, the laser was adjusted for single spot scan with 100 iterations at 820 nm, delivering ~270mJ power at the focal plane.

Myosin inhibition and analysis of neuronal survival

Intrathecal delivery of myosin inhibitor 2,3-Butanedione monoxime (BDM) was performed as previously described (*47*). Briefly, Hamilton syringe (Hamilton 80314, Hamilton, Reno, NV) with 32-gauge needle was inserted between the L2-L3 vertebrae to the subarachnoid space. Access to

the intrathecal space was confirmed by reflux of cerebrospinal fluid. Five microliter of SF containing 50mg/ml BDM was injected intrathecally 30 minutes prior to in vivo experiments.
To determine the cell death in DRG neurons, 50 µl of 1/1000 propidium iodide (PI, Molecular Probes), which stains nuclei of dead cells, was injected intravenously via the tail vein 1 hr before the microscopic imaging.

Patch clamp recordings

Patch-clamp pipettes were made of borosilicate glass (Sutter Instrument Borosilicate Glass with flament. O.D.: 1.5 mm, I.D.: 1.17 mm 10 cm Length, Novato, CA, USA). The standard extracellular bath solution contained (in mM): 130 NaCl, 2 $CaCl_2$, 10 HEPES and 13 D-glucose, pH adjusted with NaOH to 7.35. Osmolarity of the solution was 270 mOsmol/L. The pipette (internal) solution for patch-clamp recording contained (in mM): 130 K-gluconate, 5 EGTA, and 10 HEPES (270 mOsmol/L; pH 7.2) (adjusted with NaOH). The pipette resistances were about 4 – 6 MΩ. Also, the neurons were held at a potential of -70 mV. The resistance was made to be giga-seal (2 - 10 GΩ), and then the whole cell configuration was started with negative pressure. The Whole-cell patch clamp technique was used to perform current-clamp recording by using an amplifier (Axon CNS MultiClamp 700B). Low-pass-filtering at 5–10 kHz was used during data recording. Sampling rates for current and voltage records were 10–20 kHz. A Digidata 1550B interface (Axon Instruments, Foster City, CA, USA) was used for digitization of data, and a computer was used for storage and further analysis. pClamp software (version 11; Axon Instruments) was used for generation of stimulus, acquisition and off-line analysis of data.
To record from neurons during axotomy, the patch clamp rig was mounted on Palm laser microdissection microscope and after giga-seal was created a selected axon of the patched neuron was cut with laser beam as described earlier.

Calcium imaging

Cultured DRG neurons of GCaMP6s - Ai96 mice were imaged with confocal microscope before, during and immediately, then every 5 mins after axotomy. Change in green fluorescence emission was analyzed using Zen software.

Use of blocking reagents in vitro

Neurons were incubated with the blockers for one hour before microscopic manipulations except exoenzyme C3 whose incubation period was 6 hrs. All inhibitors were purchased from Sigma, except exoenzyme C3, which was obtained from Abcam.Cytochalasin E (CytE, 200 ng/ml) (*14*) and swinholide A (SWH, 500 ng/ml) (*48*) were used to depolymerize actin. Myosin activity was blocked with blebbistatin (BB, 100 µM) (*49*) and 2,3 butanedione monoxime (BDM, 50mM) (*17*). Voltage gated calcium channel subtypes L, N, P/Q, R and T were blocked with nifedipine (NIF, 10µM) (*50*), ω-conotoxin GVIA (CNX, 1µM) (*51*), ω -agatoxin-IVA(AGX, 200nM) (*52*), SNX-482(SNX, 200nM) (*52*) and mibefradil (MIB, 10µM) (*53*), respectively. To test the contribution of internally stored Ca^{++} to the shrinkage, neurons were incubated with thapsigargin (TG, 5µM) (*54*) for 30 min to irreversibly deplete the internal stores, after which the culture medium was replaced with Ca^{++} - free DMEM and then axotomy was performed.
PD150606 (50µM) (*55*) was used as a calpain inhibitor. Aquaporin channels were blocked using $HgCl_2$ (100µM) (*56*). Ras homolog gene family member A (RhoA) and its downstream effector Rho-associated protein kinase (ROCK) were inhibited with clostridium botulinum exoenzyme C3 protein (C3, 500 nM) (*57*) and Y-27632 (10 µM) (*58*), respectively.

Image Analyzes

Changes in surface area and volume of neurons were analyzed using ImageJ software. Fluorescence intensity measurements were performed with Zeiss Zen software.

Statistical analysis

IBM SPSS V24 and SAS V9.4 were used. The distribution of the data was evaluated with Kolmogorov -Smirnov test. Though some data sets had a normal distribution most of them did not, therefore non-parametric tests were used for group comparisons. The distribution of a continuous marker was compared among two or more levels of a factor of interest by using Wilcoxon-Mann-Whitney or Kruskal-Wallis tests. Change of a marker overtime was modelled through random-coefficient models using the MIXED procedure in SAS, where spatial-power of time-lag covariance structure was used to account for the correlation structure among measurements. Similarly, repeated-measures models with variance-components covariance structure were also constructed using the MIXED procedure. To estimate impact of a given predictor on the likelihood of survival, univariable Logistic regression was used and significance of the predictor was assessed through both p-values and Area Under the curve (AUC).

Competing interests: Authors declare that they have no competing interests.

Author contributions: Conceptualization: GÖ, MŞA; Methodology: GÖ, AH, MK, EE; Investigation: GÖ, MŞA, SB, ENY, CÖ, EYK, EKO, NA, NC, EE, AH; Visualization: GÖ, MŞA, ENY, EE; Funding acquisition: GÖ; Project administration: GÖ; Supervision: GÖ, EH; Writing – original draft: GÖ, Writing – review & editing: GÖ, MK, EE

Acknowledgments: This research was funded by Yüzüncü Yıl University Directorate of Scientific Research Projects, grant TF073 (GÖ) and the Scientific and Technological Research Council of Turkey (TÜBİTAK), grant 107S358 (GÖ).

Data and materials availability: All data will be deposited to an online repository upon acceptance of the manuscript for publication.

References

1. G. Mandolesi, F. Madeddu, Y. Bozzi, L. Maffei, G. M. Ratto, Acute physiological response of mammalian central neurons to axotomy: ionic regulation and electrical activity. *FASEB J* **18**, 1934-1936 (2004).
2. R. L. Rungta *et al.*, The cellular mechanisms of neuronal swelling underlying cytotoxic edema. *Cell* **161**, 610-621 (2015).
3. S. P. Yu, D. W. Choi, Na(+)-Ca2+ exchange currents in cortical neurons: concomitant forward and reverse operation and effect of glutamate. *Eur J Neurosci* **9**, 1273-1281 (1997).
4. R. M. LoPachin, E. J. Lehning, Mechanism of calcium entry during axon injury and degeneration. *Toxicol Appl Pharmacol* **143**, 233-244 (1997).

5. M. J. Hasbani, K. L. Hyrc, B. T. Faddis, C. Romano, M. P. Goldberg, Distinct roles for sodium, chloride, and calcium in excitotoxic dendritic injury and recovery. *Experimental neurology* **154**, 241-258 (1998).
6. P. Blaesse, M. S. Airaksinen, C. Rivera, K. Kaila, Cation-chloride cotransporters and neuronal function. *Neuron* **61**, 820-838 (2009).
7. S. P. Mutalik, J. Joseph, P. A. Pullarkat, A. Ghose, Cytoskeletal Mechanisms of Axonal Contractility. *Biophysical journal* **115**, 713-724 (2018).
8. G. Feng *et al.*, Imaging neuronal subsets in transgenic mice expressing multiple spectral variants of GFP. *Neuron* **28**, 41-51 (2000).
9. C. Chen *et al.*, Long-term imaging of dorsal root ganglia in awake behaving mice. *Nat Commun* **10**, 3087 (2019).
10. R. S. Scroggs, A. P. Fox, Calcium current variation between acutely isolated adult rat dorsal root ganglion neurons of different size. *J Physiol* **445**, 639-658 (1992).
11. A. Fuchs, M. Rigaud, C. D. Sarantopoulos, P. Filip, Q. H. Hogan, Contribution of calcium channel subtypes to the intracellular calcium signal in sensory neurons: the effect of injury. *Anesthesiology* **107**, 117-127 (2007).
12. R. S. Scroggs, A. P. Fox, Multiple Ca2+ currents elicited by action potential waveforms in acutely isolated adult rat dorsal root ganglion neurons. *J Neurosci* **12**, 1789-1801 (1992).
13. E. Carbone, H. D. Lux, A low voltage-activated, fully inactivating Ca channel in vertebrate sensory neurones. *Nature* **310**, 501-502 (1984).
14. G. Ruthel, P. J. Hollenbeck, Growth cones are not required for initial establishment of polarity or differential axon branch growth in cultured hippocampal neurons. *J Neurosci* **20**, 2266-2274 (2000).
15. M. R. Bubb, I. Spector, A. D. Bershadsky, E. D. Korn, Swinholide A is a microfilament disrupting marine toxin that stabilizes actin dimers and severs actin filaments. *J Biol Chem* **270**, 3463-3466 (1995).
16. J. Limouze, A. F. Straight, T. Mitchison, J. R. Sellers, Specificity of blebbistatin, an inhibitor of myosin II. *J Muscle Res Cell Motil* **25**, 337-341 (2004).
17. M. J. Siegman *et al.*, Comparison of the effects of 2,3-butanedione monoxime on force production, myosin light chain phosphorylation and chemical energy usage in intact and permeabilized smooth and skeletal muscles. *J Muscle Res Cell Motil* **15**, 457-472 (1994).
18. G. Zhang, J. Hu, W. Rodemer, S. Li, M. E. Selzer, RhoA activation in axotomy-induced neuronal death. *Experimental neurology* **306**, 76-91 (2018).
19. A. Hall, Rho GTPases and the actin cytoskeleton. *Science* **279**, 509-514 (1998).
20. Q. Lu *et al.*, RhoA/mDia-1/profilin-1 signaling targets microvascular endothelial dysfunction in diabetic retinopathy. *Graefes Arch Clin Exp Ophthalmol* **253**, 669-680 (2015).
21. Y. A. Miroshnikova *et al.*, Calcium signaling mediates a biphasic mechanoadaptive response of endothelial cells to cyclic mechanical stretch. *Mol Biol Cell* **32**, 1724-1736 (2021).
22. M. P. Stewart *et al.*, Hydrostatic pressure and the actomyosin cortex drive mitotic cell rounding. *Nature* **469**, 226-230 (2011).
23. P. S. Vosler, C. S. Brennan, J. Chen, Calpain-mediated signaling mechanisms in neuronal injury and neurodegeneration. *Mol Neurobiol* **38**, 78-100 (2008).
24. M. B. Bevers, R. W. Neumar, Mechanistic role of calpains in postischemic neurodegeneration. *J Cereb Blood Flow Metab* **28**, 655-673 (2008).

25. M. Krieg, A. R. Dunn, M. B. Goodman, Mechanical control of the sense of touch by beta-spectrin. *Nat Cell Biol* **16**, 224-233 (2014).
26. S. L. Chan, M. P. Mattson, Caspase and calpain substrates: roles in synaptic plasticity and cell death. *J Neurosci Res* **58**, 167-190 (1999).
27. F. Yellin *et al.*, Electromechanics and Volume Dynamics in Nonexcitable Tissue Cells. *Biophysical journal* **114**, 2231-2242 (2018).
28. M. C. Papadopoulos, A. S. Verkman, Aquaporin water channels in the nervous system. *Nat Rev Neurosci* **14**, 265-277 (2013).
29. K. L. Tucker, M. Meyer, Y. A. Barde, Neurotrophins are required for nerve growth during development. *Nat Neurosci* **4**, 29-37 (2001).
30. S. Agarwala, R. E. Kalil, Axotomy-induced neuronal death and reactive astrogliosis in the lateral geniculate nucleus following a lesion of the visual cortex in the rat. *J Comp Neurol* **392**, 252-263 (1998).
31. K. M. Rich, S. P. Disch, M. E. Eichler, The influence of regeneration and nerve growth factor on the neuronal cell body reaction to injury. *J Neurocytol* **18**, 569-576 (1989).
32. L. Li *et al.*, Characterization of spinal motoneuron degeneration following different types of peripheral nerve injury in neonatal and adult mice. *J Comp Neurol* **396**, 158-168 (1998).
33. T. Ota, H. Hara, N. Miyawaki, Brain-derived neurotrophic factor inhibits changes in soma-size of retinal ganglion cells following optic nerve axotomy in rats. *J Ocul Pharmacol Ther* **18**, 241-249 (2002).
34. D. M. Armstrong *et al.*, Response of septal cholinergic neurons to axotomy. *J Comp Neurol* **264**, 421-436 (1987).
35. K. M. Giehl, W. Tetzlaff, BDNF and NT-3, but not NGF, prevent axotomy-induced death of rat corticospinal neurons *in vivo*. *Eur J Neurosci* **8**, 1167-1175 (1996).
36. J. Brown, P. C. Bridgman, Role of myosin II in axon outgrowth. *J Histochem Cytochem* **51**, 421-428 (2003).
37. X. Wan, J. A. Harris, C. E. Morris, Responses of neurons to extreme osmomechanical stress. *J Membr Biol* **145**, 21-31 (1995).
38. H. Zhang, A. S. Verkman, Aquaporin-1 water permeability as a novel determinant of axonal regeneration in dorsal root ganglion neurons. *Experimental neurology* **265**, 152-159 (2015).
39. B. Buffoli, E. Borsani, R. Rezzani, L. F. Rodella, Chronic constriction injury induces aquaporin-2 expression in the dorsal root ganglia of rats. *J Anat* **215**, 498-505 (2009).
40. A. S. Verkman, M. O. Anderson, M. C. Papadopoulos, Aquaporins: important but elusive drug targets. *Nat Rev Drug Discov* **13**, 259-277 (2014).
41. E. R. de Moraes, C. Kushmerick, L. A. Naves, Morphological and functional diversity of first-order somatosensory neurons. *Biophys Rev* **9**, 847-856 (2017).
42. B. M. Gaub *et al.*, Neurons differentiate magnitude and location of mechanical stimuli. *Proc Natl Acad Sci U S A* **117**, 848-856 (2020).
43. M. Okabe, M. Ikawa, K. Kominami, T. Nakanishi, Y. Nishimune, 'Green mice' as a source of ubiquitous green cells. *FEBS Lett* **407**, 313-319 (1997).
44. L. Madisen *et al.*, Transgenic mice for intersectional targeting of neural sensors and effectors with high specificity and performance. *Neuron* **85**, 942-958 (2015).
45. L. Vong *et al.*, Leptin action on GABAergic neurons prevents obesity and reduces inhibitory tone to POMC neurons. *Neuron* **71**, 142-154 (2011).
46. G. Ozturk *et al.*, Two distinct types of dying back axonal degeneration *in vitro*. *Neuropathol Appl Neurobiol* **39**, 362-376 (2013).

47. N. Ogawa, T. Terashima, K. Oka, L. Chan, H. Kojima, Gene therapy for neuropathic pain using dorsal root ganglion-targeted helper-dependent adenoviral vectors with GAD67 expression. *Pain Rep* **3**, e695-e695 (2018).
48. J. Bourne, J. R. Morgan, V. A. Pieribone, Actin polymerization regulates clathrin coat maturation during early stages of synaptic vesicle recycling at lamprey synapses. *J Comp Neurol* **497**, 600-609 (2006).
49. G. Gallo, Myosin II activity is required for severing-induced axon retraction *in vitro*. *Experimental neurology* **189**, 112-121 (2004).
50. N. W. Bellono *et al.*, Enterochromaffin Cells Are Gut Chemosensors that Couple to Sensory Neural Pathways. *Cell* **170**, 185-198 e116 (2017).
51. F. A. Abdulla, P. A. Smith, Axotomy- and autotomy-induced changes in Ca2+ and K+ channel currents of rat dorsal root ganglion neurons. *J Neurophysiol* **85**, 644-658 (2001).
52. S. S. Murali *et al.*, High-voltage-activated calcium current subtypes in mouse DRG neurons adapt in a subpopulation-specific manner after nerve injury. *J Neurophysiol* **113**, 1511-1519 (2015).
53. Z. H. Pan, H. J. Hu, P. Perring, R. Andrade, T-type Ca(2+) channels mediate neurotransmitter release in retinal bipolar cells. *Neuron* **32**, 89-98 (2001).
54. T. Adasme, A. Paula-Lima, C. Hidalgo, Inhibitory ryanodine prevents ryanodine receptor-mediated Ca(2)(+) release without affecting endoplasmic reticulum Ca(2)(+) content in primary hippocampal neurons. *Biochem Biophys Res Commun* **458**, 57-62 (2015).
55. L. Van den Bosch *et al.*, An alpha-mercaptoacrylic acid derivative (PD150606) inhibits selective motor neuron death via inhibition of kainate-induced Ca2+ influx and not via calpain inhibition. *Neuropharmacology* **42**, 706-713 (2002).
56. H. Zhang, A. S. Verkman, Aquaporin-1 tunes pain perception by interaction with Na(v)1.8 Na+ channels in dorsal root ganglion neurons. *J Biol Chem* **285**, 5896-5906 (2010).
57. A. Rohrbeck, L. von Elsner, S. Hagemann, I. Just, Uptake of clostridium botulinum C3 exoenzyme into intact HT22 and J774A.1 cells. *Toxins (Basel)* **7**, 380-395 (2015).
58. A. S. Maddox, K. Burridge, RhoA is required for cortical retraction and rigidity during mitotic cell rounding. *J Cell Biol* 160, 255-265 (2003).